



## Research Article

# A microfluidic approach to studying the injection flow of concentrated albumin solutions

Alfredo Lanzaro<sup>1,2</sup> 

Received: 1 October 2020 / Accepted: 13 August 2021

Published online: 24 August 2021

© The Author(s) 2021 [OPEN](#)

## Abstract

Subcutaneous injection by means of prefilled syringes allows patients to self-administrate high-concentration (100 g/L or more) protein-based drugs. Although the shear flow of concentrated globulins or monoclonal antibodies has been intensively studied and related to the injection force proper of SC processes, very small attention has been paid to the extensional behavior of this category of complex fluids. This work focuses on the flow of concentrated bovine serum albumin (BSA) solutions through a microfluidic “syringe-on-chip” contraction device which shares some similarities with the geometry of syringes used in SC self-injection. By comparing the velocity and pressure measurements in complex flow with rheometric shear measurements obtained by means of the “Rheo-chip” device, it is shown that the extensional viscosity plays an important role in the injection process of protinaceous drugs.

## Article Highlights

- A microfluidic “syringe on chip” device mimicking the injection flow of protinaceous drugs has been developed.
- The velocity field of concentrated BSA solutions through the “syringe on chip” is Newtonian-like.
- The extensional viscosity of concentrated protein solutions should also be considered when computing injection forces through needles.

**Keywords** Biopharmaceuticals · Concentrated protein solutions · Microfluidics · Complex flows · Extensional rheometry

## 1 Introduction

Macromolecules such as monoclonal antibodies (mAbs) are increasingly being used for treating a large variety of diseases, including immunodeficiency, leukemia and arthritis [17], while globular proteins such as recombinant serum albumin are often employed as drug stabilizers [28, 59]. Subcutaneous (SC) injection by means of prefilled

syringes coupled with autoinjector devices constitutes a viable alternative to intravenous delivery, as it allows the patients to self-administrate the protinaceous drug at home. Perceived pain and back pressure typically limit the highest deliverable volume to 1.5 mL [37, 58, 62]; therefore, biopharmaceuticals need to be concentrated above 100 g/L in order for the drug to be effective. Such large values of protein concentrations typically translate into

✉ Alfredo Lanzaro, [alfredo.lanzaro@gzhu.edu.cn](mailto:alfredo.lanzaro@gzhu.edu.cn) | <sup>1</sup>Present Address: Institute for Systems Rheology, Guangzhou University, Guangzhou 510006, People's Republic of China. <sup>2</sup>School of Chemical Engineering and Analytical Science, Faculty of Engineering and Physical Sciences, University of Manchester, Manchester M13 9PL, UK.



large solution viscosity (up to 1 Pa s [2, 63]) as well as into shear thinning behavior [8, 11, 18, 68] at the shear rates typical of SC injection ( $10^4 \leq \dot{\gamma} \leq 10^5 \text{ s}^{-1}$  for 27-G needle syringes, see [1]).

Several previous works have produced a calculation of the injection force of concentrated mAbs through syringes by assuming either Newtonian or shear-thinning viscosity [1, 7, 48]. It must however be observed that the flow of protein solutions through needles can be considered as a complex flow, because it contains not only a shear component, but also a well-defined extensional contribution which is localized in the contraction part between the syringe barrel and the needle. Thus, in order to develop a complete understanding of the origin of the forces arising when a biopharmaceutical drug is delivered by means of SC injection, one must characterize not only the shear, but also the extensional viscosity of concentrated protein solutions. While there is a large amount of works which focus on bulk shear viscosity [29, 36, 53, 68], high-frequency viscoelasticity [42, 43, 65] or interfacial shear rheometry [26, 57] of dense protein solutions, very little attention has so far been paid to the elongational behavior of this category of complex fluids.

The extensional viscosity of complex fluids is directly related to the amount of deformation underwent by macromolecules under flow. Following de Gennes' work [10], a polymer in extensional flow undergoes a transition from coiled to uncoiled state if it is deformed with a strain rate whose magnitude is comparable to the inverse of the longest polymer relaxation time, and for a long enough time such that a sufficient amount of strain can be accumulated. For example,  $\lambda$ -bacteriophage DNA has a relaxation time of approximately 0.1 s [45], and hence it reaches the uncoiled state if extensional rates of  $10 \text{ s}^{-1}$  or above are applied. While there is a general consensus in the literature on the flow conditions that need to be achieved in order to stretch DNA and linear polymer chains, the data related to proteins are more controversial. Jaspe and Hagen [27] estimated that horse cytochrome unravels under purely extensional flow at strain rates of  $10^7 \text{ s}^{-1}$  or above. Churchich et al. [9] suggest that also the relaxation time of a much larger globulin such as bovine serum albumin (BSA) is on the order of  $10^{-7} \text{ s}$ . This is in contrast to the experimental work of Bekard et al. [5], which suggest that bovine serum albumin (BSA) unfolds in Couette flows at shear rates as low as  $10^2 \text{ s}^{-1}$ . By means of a microfluidic device, Schneider [54] demonstrated that the von Willebrand factor, a protein commonly found in human blood, can unravel at shear rates of about  $10^3 \text{ s}^{-1}$ . Computer simulations [60, 61] showed that the unraveling under shear flow of ubiquitin and integrin gives rise to many more intermediates than in the case of homopolymers. The dynamics of unraveling also depend on whether the

protein is anchored or not, and on which specific protein site is anchored. More recently, Dobson et al. [13] showed that BSA and monoclonal antibodies can also aggregate when they undergo multi-pass extensional flow at strain rates  $\dot{\epsilon} \cong 10^4 \text{ s}^{-1}$ . The authors suggest that the aggregation of protein molecules at large extensional rates is caused by flow-driven protein unfolding, which is in turn related to strong hydrodynamic forces.

The advent of microfluidics has made it possible to study flow regimes which could not be previously investigated. Due to characteristic sizes of just a few microns, microfabricated devices allow for fluids to be tested under very large ( $\dot{\gamma} \geq 10^4 \text{ s}^{-1}$ ) rates of deformation, while Reynolds numbers (hence inertial effects) are almost negligible. When macromolecular solutions are subjected to large deformation rates in microscopic flows through abrupt [30, 35, 49, 50] and hyperbolic contractions [32] or "cross-slots" [3, 24, 33], nonlinear flow effects such as asymmetries in the flow field and vortex development are often witnessed. While a considerable amount of effort has been spent in studying microscopic flows of macromolecular fluids such as polymers, DNA and other biopolymers [19–21, 23], or wormlike micellar solutions [22, 44, 69], very little attention has so far been paid to the behavior of concentrated protein solutions at high deformation rate, complex flow conditions which mimic practical processes. It is then natural to ask if the flow-induced protein unraveling and/or aggregation phenomena discussed above can lead to nonlinear flow effects similar to what has been previously observed for other types of macromolecules.

In the present work, the commonly made assumption that the injection force of proteinaceous drugs is made only by a purely shear contribution is critically assessed. This is done by means of a microfluidic platform which mimics the flow behavior of concentrated protein solutions when flowing through syringes. Three BSA solutions in a pH = 7.0 buffer condition and at  $c_2 = 100, 200$  and  $300 \text{ g/L}$  were used here. Such concentrations are above the physiological value ( $7 \times 10^{-4} \text{ M}$ , equivalent to  $c_2 \approx 50 \text{ g/L}$ ) typically found in human blood [14]. Nevertheless, BSA solutions at this pH and over this range of  $c_2$  are expected to have a similar shear and extensional viscosity with respect to that of mAbs-based biopharmaceuticals [53]. The microscopic geometries employed here are straight channel and a "syringe-on-chip" device consisting in several sudden planar contractions with same contraction ratio as those found in 26-G, 27-G and 30-G syringe needles. From the first geometry, the steady shear viscosity  $\eta(\dot{\gamma})$  corresponding to a range of deformation rates ( $10 \text{ s}^{-1} \leq \dot{\gamma} \leq 10^4 \text{ s}^{-1}$ ) comparable with that of the syringe injection process is extracted. From the "syringe-on-chip" geometry, the velocity and local strain rate fields within a similar range of nominal deformation rates are measured

by means of particle-image velocimetry (PIV) [39, 41], so that it is verified whether the flow of the BSA solutions retains a Newtonian character. Finally, the extra pressure drops from the “syringe-on-chip” device are critically compared with the results obtained from the steady shear flow measurements, so that the relative importance of shear and extensional viscosity in the overall injection force can be assessed.

## 2 Materials

BSA (Cat. no. A7906) was obtained from Sigma-Aldrich. The protein was initially dissolved at a concentration  $c_2 = 300$  g/L in a pre-filtered buffer made by NaCl (145 mM), sodium octanoate (8 mM) and Tween 80 (0.05 g/L) at a pH = 7.0 and let to dissolve for 72 h at 5 °C. The initial BSA sample was filtered with a 0.22-microns filter (Anotop 10 filters, GE Healthcare, Piscataway, CA) to remove irreversible aggregates, and then fresh buffer was used for all subsequent dilutions up to the desired  $c_2 = 100, 200$  or 300 g/L. The concentration of the protein samples was confirmed by a UV-1600PC spectrophotometer (VWR) operating at a wavelength of 280 nm. The small-angle X-ray scattering (SAXS) measurements performed by Sønderby et al. [59] on recombinant serum albumin, a globulin very similar to BSA, demonstrated that protein–protein interactions are repulsive under the chosen buffer conditions.

## 3 Experimental methodology

### 3.1 Rheo-chip platform

All microfluidic experiments presented in this work were run by means of the “Rheo-chip” platform [67]. It consists of a series of microchannels made in polymethylmethacrylate (PMMA) by Epigem Ltd (Redcar, TS, UK). Each microchip features a delivery module where inlets, outlets and pressure taps are obtained. Pressure measurements were taken by means of Honeywell strain gauge sensors 26PCGFM6G (range 0–250 psi). The transient pressure signals were collected at 50 Hz by a cDAQ data acquisition system (National Instruments) and a LabVIEW software. The flow through microfluidic devices was controlled by means of a Nexus 6000 high force syringe pump (Chemyx Inc, Stafford, Tx) equipped with a 1-mL glass syringe (SGE Analytical, ID = 4.5 mm). Note that, differently from other microfluidics-based rheometric techniques available elsewhere [46], the Rheo-chip technology employs replaceable pressure sensors, so that only the microfluidic chips need to be replaced if microchannels are clogged. This

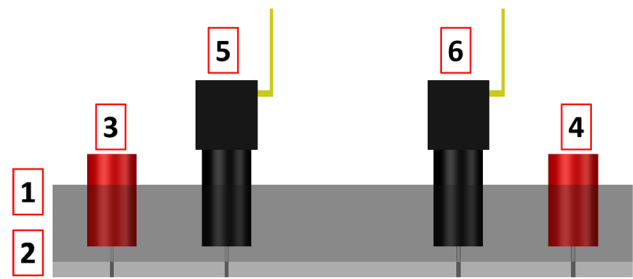


**Fig. 1** Schematic diagram of a “Rheo-chip” microdevice. 1 Delivery module. 2 Microfluidic flow geometry. 3 Inlet. 4 Outlet. 5 and 6 Honeywell pressure sensors

makes the rheometric characterisation of precious materials such as concentrated protein solutions much more cost-effective. The schematic diagrams of the “Rheo-chip” coupled with the pressure sensors are given in Fig. 1.

### 3.2 Shear viscosity measurements

The steady shear viscosities of the model protein solutions were measured by means of Rheo-chips featuring a straight channel with width  $w_c = 800$   $\mu\text{m}$ , depth  $h_{\text{nominal}} = 50$   $\mu\text{m}$  and length  $L = 30$  mm. Two pressure taps were located along the microchannel at a distance of  $L = 30$  mm from each other, far away from the inlet and outlet, to measure the overall pressure drop  $\Delta P_s$ . The pressure signals were collected by imposing an initial flow rate  $Q_{\text{max}} = 10$  mL/h and then waiting for the signal to reach a steady-state value. The flow rate was then reduced to 8 mL/h, and the procedure was repeated until a steady-state pressure drop corresponding to a flow rate  $Q_{\text{min}} = 0.25$  mL/h was measured [46]. For all samples studied in this paper, the nominal shear rate at walls is defined as

$$\dot{\gamma}_N = \frac{2Q}{h_{\text{true}}^2 w_c}, \quad (1)$$

where  $h_{\text{true}}$  is found by fitting the steady-state pressure drop measurements of DI water with the analytical prediction for Newtonian flows through rectangular ducts given by White [64]. The corresponding shear viscosity is

$$\eta_N = \eta_{\text{buffer}} K \frac{\Delta P_s(\dot{\gamma})}{\dot{\gamma}}, \quad (2)$$

where the calibration coefficient  $\frac{1}{K} = \frac{\Delta P_{\text{buffer}}}{\dot{\gamma}}$  is obtained by averaging the ratios between steady-state pressure drops of buffer and the corresponding shear rates, and  $\eta_{\text{buffer}} \cong 1$  mPa s is the shear viscosity of buffer as measured by a TA

ARES-G2 rheometer equipped with cone and plate measurement tool. The overall measurement time for each sample was 20 mins, approximately, and an amount of sample between 0.6 and 1 mL was used for each measurement. The impact of viscous heating on the rheometric measurements was estimated by the Nahme–Griffith number

$$Na = \frac{\eta_0 \beta d_h^2 \dot{\gamma}^2}{\kappa T}, \tag{3}$$

where  $\kappa \approx 0.5918 \text{ W/(m K)}$  is the thermal conductivity of buffer and  $\beta = \frac{T}{\eta_{\text{buffer}}} \left| \frac{d\eta}{dT} \right|_{T=T_0} \approx 2.6$  is the logarithmic derivative of shear viscosity of buffer with temperature  $T$  evaluated at  $T=T_0 = 25^\circ\text{C}$ . It expresses the ratio between the heat generated by viscous heating of samples and the heat released by thermal diffusion at the surface of the microchannels [46].  $Na$  resulted to be  $\leq 10^{-5}$  for all the samples and shear rates studied here, which systematically excludes the influence of thermal effects.

### 3.3 “Syringe-on-chip” microdevices

The two “syringe-on-chip” microdevices that are used in this work are presented in Fig. 2. They consist of planar sudden contraction devices with an upstream width  $w_u = 800 \mu\text{m}$ , channel depth  $h = 50 \mu\text{m}$  and downstream widths  $w_d = 47$  and  $38 \mu\text{m}$ . The corresponding contraction ratios  $\beta=17.02$  and  $21.05$  are the same as what is typically found in syringes where the plunger diameter is 4.5

mm and the needle is a 26G or 27G [66]. Hence, from here onwards such microcontractions will be labeled as “26G” and “27G” geometry, respectively. Note that, due to fact that real syringes have axisymmetric instead of planar abrupt geometries, the flow through the syringe-on-chip devices feature lower Hencky strains  $\epsilon_H = \ln \beta$  compared to real syringes case, where  $\epsilon_H = 2 \ln \beta$ . Each flow geometry contains a slot for a pressure sensor as in the figure. The outlet of each microchannel is connected to a fluid reservoir by means of a stainless steel tube with length  $L_{\text{tube}} = 100 \text{ mm}$  and inner diameter  $ID = 1/16 \text{ inches}$  (Cat. No. 56720-U, Sigma-Aldrich). The total pressure drop  $\Delta P_{\text{total}}$  measured by the sensor is related to the pressure drop  $\Delta P$  across the device by  $\Delta P_{\text{total}} = \Delta P + \Delta P_{\text{tube}}$ , where  $\Delta P_{\text{tube}} = \frac{128 \mu L Q}{\pi ID^4}$  is estimated by means of the Hagen–Poiseuille law. The  $\Delta P_{\text{tube}}$  contribution resulted to be 5% or less of the total pressure drop. The details of the flow geometries are given in Table 1. The flow of the concentrated BSA solutions in complex geometry is characterized in terms of the Reynolds number  $Re$

$$Re = \frac{\rho \langle v_d \rangle D_h}{\eta_0}, \tag{4}$$

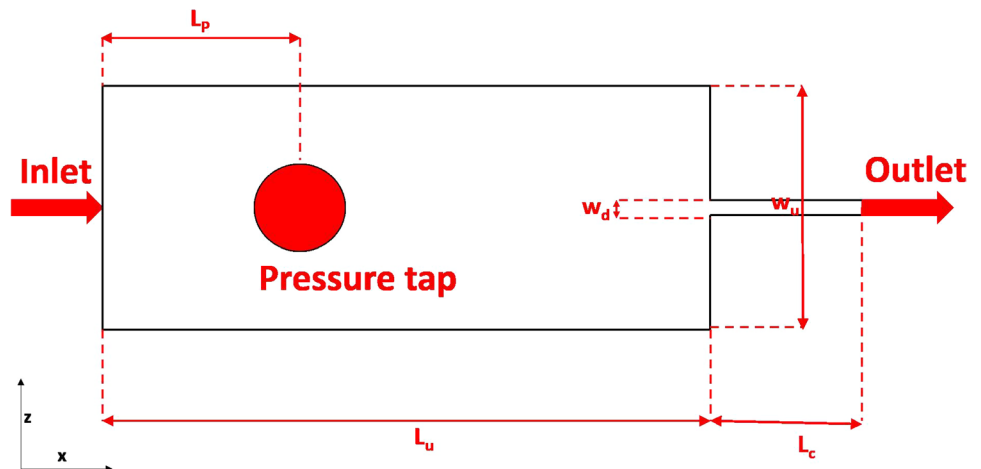
where  $\langle v_d \rangle$ ,  $\rho \approx 1000 \text{ g/L}$  and  $\eta_0$  are the average speed in the downstream channel, the fluid density and zero-shear viscosity, respectively, and  $D_h = \frac{2hw_d}{h+w_d}$  is the hydraulic diameter of the downstream channel. In addition to  $Re$ , the Péclet number

**Table 1** The details of “syringe-on-chip” flow geometries

Flow cell	$w_u$ [ $\mu\text{m}$ ]	$w_d$ [ $\mu\text{m}$ ]	$h$ [ $\mu\text{m}$ ]	$\alpha$	$\beta$	$\epsilon_H$
26G	800	47	50	20	17.02	2.83
27G	800	38	50	20	21.05	3.05

$\alpha$  and  $\beta$  denote the upstream aspect ratio and contraction ratio, respectively.  $\epsilon_H = \ln \beta$  is the Hencky strain

**Fig. 2** Schematic diagram of the “syringe-on-chip” microfluidic geometry. The dimensions  $w_u$  and  $w_d$  are given in Table 1, and  $L_p=14 \text{ mm}$ ,  $L_u = 32 \text{ mm}$  and  $L_c = 12 \text{ mm}$



$$Pe = \frac{\tau_D}{\tau_F} \quad (5)$$

expresses the ratio between the characteristic timescales of flow,  $\tau_F = \frac{1}{\dot{\gamma}} = \frac{w_d}{2\langle v_d \rangle}$  and Brownian diffusion [34]. The diffusion time is  $\tau_D = \frac{d_h^2}{D_L^S}$ , where  $d_h = 7$  nm is the hydrodynamic diameter of BSA [4], and  $D_L^S$  is the longtime self-diffusion coefficient of the BSA molecule, which is estimated by the generalized Stokes–Einstein relationship [51] as

$$D_L^S = \frac{k_B T}{3\pi\eta_0 d_h}, \quad (6)$$

with  $k_B$  and  $T \approx 25$  °C being the Boltzmann constant and temperature, respectively.

### 3.4 Particle-image velocimetry and data analysis method

Velocity fields at the center plane of the “syringe-on-chip” flow channels were measured by a  $\mu$ -PIV system (TSI Instruments Ltd, USA). It consists of a pulsed Nd:YAG laser emitting at a wavelength of 532 nm, a Nikon TE2000-E fluorescent microscope, and an 8 Hz CCD camera with a resolution of  $1280 \times 1024 \times 12$  bits. A Nikon objective lens with magnification  $M = 10X$  and numerical aperture  $NA = 0.3$  was used. In Fig. 3, a schematic diagram of the “syringe-on-chip” device coupled with the PIV system is shown.

The BSA solutions were seeded with 0.01 wt% epifluorescent particles (diameter  $d_p = 1.0$   $\mu$  m,  $Ex_{max}/Em_{max} = 542/612$ , Duke Scientific Co.). For the above setup, the estimated measurement depth is 26  $\mu$ m, equivalent to 52% of the channel depth [38]. All velocity measurements were taken after the pressure drop reached a steady value. Velocity fields were obtained by means of a Nyquist grid engine and a

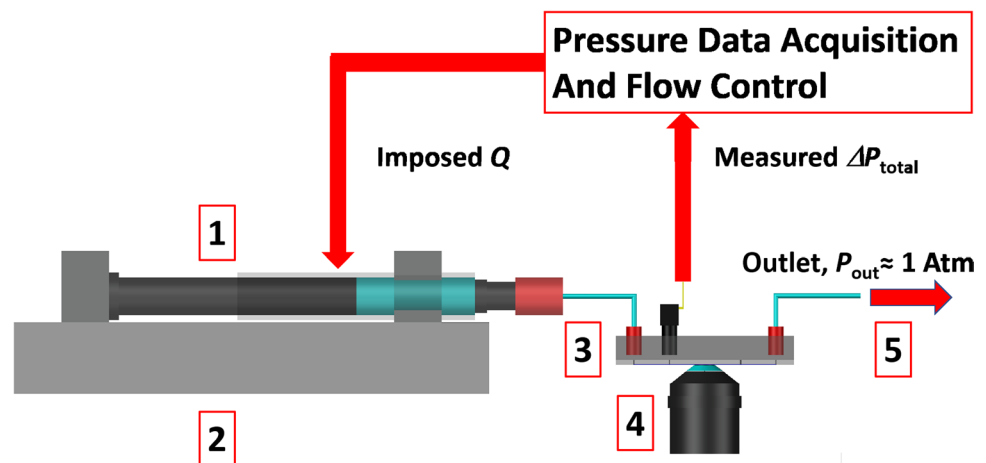
cross-correlation PIV algorithm supplied by TSI. All the  $\mu$ -PIV measurements presented in this work were performed at the middleplane of flow channel, determined by positioning the focus plane at half of the depth between the top and bottom surfaces of the microchannel, using a high-precision y-axis linear motor with step resolution 50 nm. The error in the velocity measurements is about 12–16% below the true value. This systematic error could be reduced where a higher magnification objective lens with a larger  $NA$  used. The details of the  $\mu$ -PIV techniques can be found in [39, 52]. All the velocity fields presented in this work were obtained by averaging 50 consecutive instantaneous velocity fields, corresponding to an overall measurement time of 12.5 s. From the measured two-dimensional planar velocity field  $\underline{v} = \underline{v}(x, z)$ , the largest eigenvalue  $\lambda_1$  of the strain rate tensor  $\underline{D} = \frac{1}{2}(\nabla \underline{v} + \nabla \underline{v}^T)$  is then evaluated to construct the local extensional rate field  $\dot{\epsilon}_1(x, z)$ . The uncertainty about the PIV velocity measurements is about 12–16%. More information on the computation of  $\dot{\epsilon}_1(x, z)$  can be found in [33].

## 4 Results

### 4.1 BSA solutions under steady shear flow

The shear viscosity of the BSA solutions is plotted as a function of the shear rate  $200 \text{ s}^{-1} \leq \dot{\gamma} \leq 2 \times 10^4 \text{ s}^{-1}$  in Fig. 4a. The viscosity curve of a weakly shear thinning, semi-dilute polyacrylamide (PAAm) solution [30] is also shown for a comparison. The rheograms of BSA appeared to be essentially flat, which is attributed to  $Pe$  being below unity throughout the imposed range of  $\dot{\gamma}$  (see Fig. 4b). A recent work [12] demonstrated that

**Fig. 3** Schematic diagram of a typical “syringe-on-chip” experimental setup. The LabVIEW-based data acquisition platform allows to impose a flow rate  $Q$  to the syringe pump, and to measure the total pressure drop  $\Delta P_{total}$  from the pressure sensor. 1 Sample-filled glass syringe. 2 Syringe pump. 3 “Syringe-on-chip” microdevice. 4 Magnification lens. 5 Outlet piping



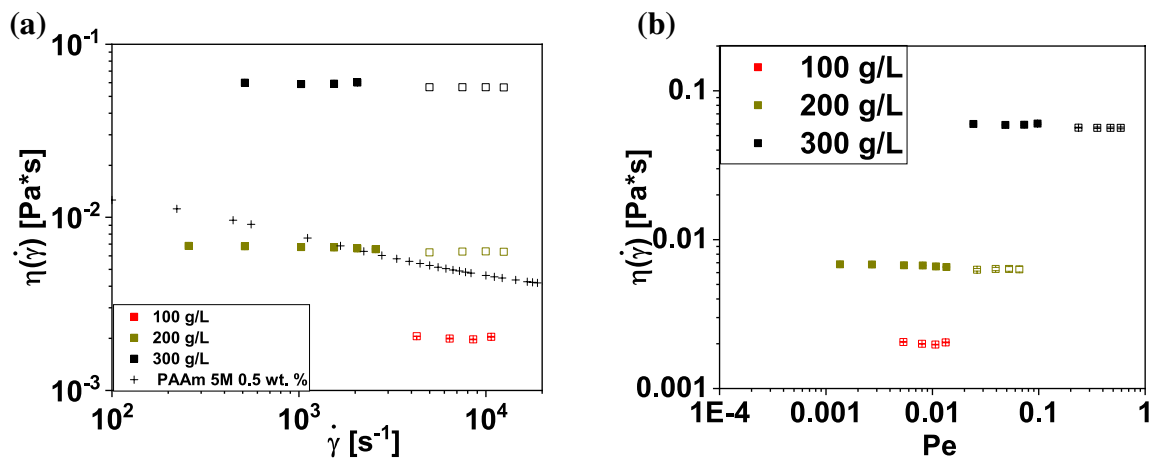


**Fig. 4** Shear viscosities plotted vs shear rate (a) and vs the Péclet number (b) for the 100, 200 and 300 g/L BSA solutions. Filled and empty symbols indicate measurements taken with the 800

and 200  $\mu m$  Rheo-chip, respectively. In a, the shear viscosity of a 0.5 wt% solution of 5M polyacrylamide is also shown for a comparison [30]

concentrated lysozyme solutions at 5 °C undergo shear thinning over a similar range of  $\dot{\gamma}$  than what studied here. Such nonlinear effect was attributed to short-range attractive interactions, which lead to the formation of intermediate structures with a size larger than that of the monomer. The absence of shear thinning effect suggests that no intermediate structures are formed in the BSA solutions studied in this work. Unlike the BSA conditions studied here, mAb solutions are known to display shear-thinning effect even at  $Pe \ll 1$  [11, 18, 47]. In a recent work, the Rheo-chip technique adopted here has been used for studying the formulation dependence of  $\eta_0$  of concentrated solutions of two mAbs [56]. Moreover, in a future work the relationship between the protein–protein interactions and the shear thinning behavior of concentrated solutions of the same two mAbs will be investigated in detail.

#### 4.2 Velocity and local extensional rate fields in “syringe on chip”

In Fig. 5a, the PIV-measured, planar velocity field of the  $Re = 0.09$ ,  $Pe = 0.24$  flow of the 300 g/L BSA solution through the 26-G microchannel is shown, to demonstrate its Newtonian-like behavior. To further assess the linearity of the flow field, the  $\dot{\epsilon}(x, z)$  field of the same BSA solution is plotted in Fig. 5b. The maximum measured extensional rate is localized near the contraction throat and resulted to be  $\approx 1500 s^{-1}$ . Such strain rate is one order of magnitude above the threshold value for BSA unfolding ( $10^2 s^{-1}$ ) reported by Bekard et al. [5], and about 10 times below the strain rate at which extensional flow-driven aggregation of BSA in multi-pass extensional flow occurs [13]. The maximum measured

value of the extensional rate is located at the point  $(x, z) \approx (0, 0)$ . This is a further indication of the absence nonlinear flow effects, like steady viscoelastic flows or lip vortices [50], which are typically revealed by the maximum strain rate point being located at  $x = 0$  and  $|\frac{z}{w_d}| > 0.5$ , that is, outside the lips of the contraction [6, 31, 32]. Therefore, these results indicate that the BSA molecules did not unfold under the existing flow conditions or, even if any unfolding event occurred, it was not released a sufficient amount of elastic energy to trigger the onset of non-Newtonian flow effects.

In Fig. 6, the dimensionless axial velocity profiles  $\frac{v(x=0)}{\langle v_u \rangle}$ , where  $\langle v_u \rangle = \frac{Q}{hw_u}$  is the mean flow velocity in the upstream channel, are shown for  $0.2 mL/h \leq Q \leq 1 mL/h$ . The velocity profiles overlap within the range of measured  $Re$ , which again indicates that the flow field is always Newtonian-like within the range of explored flow rates.

#### 4.3 Pressure measurements through “syringe on chip”

In Fig. 7, the pressure measurements through the 26-G microcontraction are plotted as a function of  $Re$  for the buffer as well as for the 100 g/L and the 200 g/L BSA solutions. The experimental data are compared with the corresponding steady-state pressure drop contributions  $\Delta P_{shear}$ , which are estimated as

$$\Delta P_{shear} = L_1 \frac{dP}{dz}(\alpha_1) + L_2 \frac{dP}{dz}(\alpha_2), \tag{7}$$

where the pressure gradients  $\frac{dP}{dz}(\alpha_i)$  are computed according to the analytical prediction for Newtonian flows through rectangular ducts given to White [64],

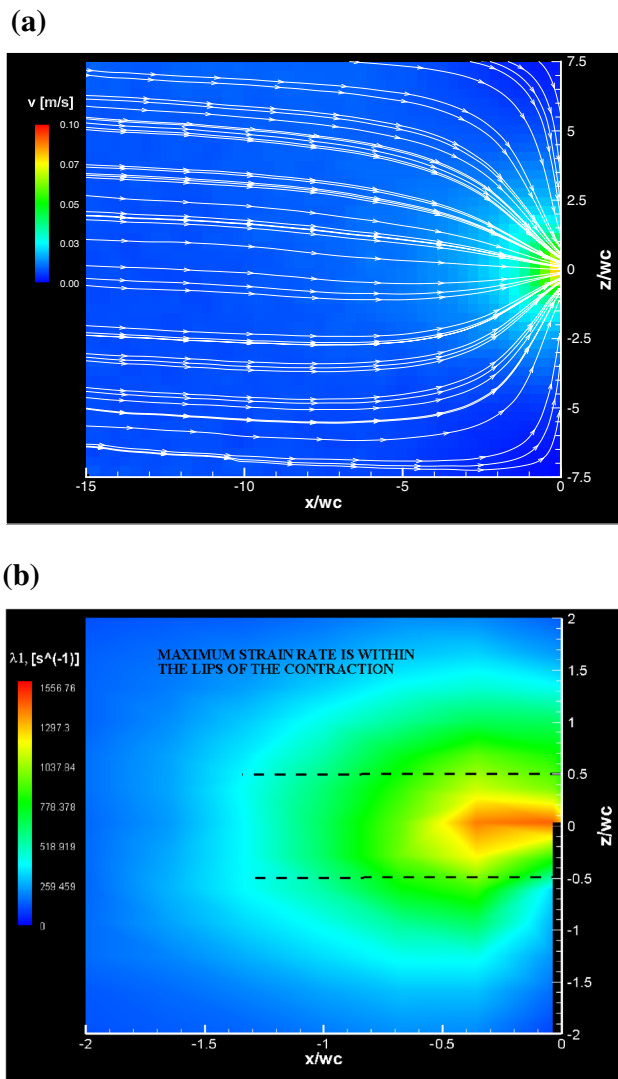


Fig. 5 Velocity field (a) and local strain field (b) for a  $Re = 0.09$ ,  $Pe = 0.24$  flow of a 300 g/L BSA solution through a “26-G” microchannel. The origin  $(x, z) = (0, 0)$  is located in the middle of the contraction throat

$$\frac{dP}{dz}(\alpha_i) = \frac{3\eta_0}{4w_c h^3 \alpha_i^4} \frac{Q}{1 - \frac{192\alpha_i}{\pi^5 K}} \tag{8}$$

where  $\alpha_1 = \frac{w_u}{h}$ ,  $\alpha_2 = \frac{w_d}{h}$ , and  $K = \sum_{n=1,3,5,\dots}^{+\infty} \frac{\tanh(\frac{n\pi}{2\alpha_i})}{n^5}$ . Such prediction ignores entry and exit effects and assumes that the flow instantaneously reaches the fully developed profile in both the upstream and downstream regions. The total pressure drop across the microchannels is above the purely shear contribution for all the BSA solutions. Such discrepancy is attributed to extensional effects across the sudden contraction, which are in turn related to the extensional viscosity of the model BSA solutions [21, 23, 33]. Due to the fact that the flow geometry used here is a sudden

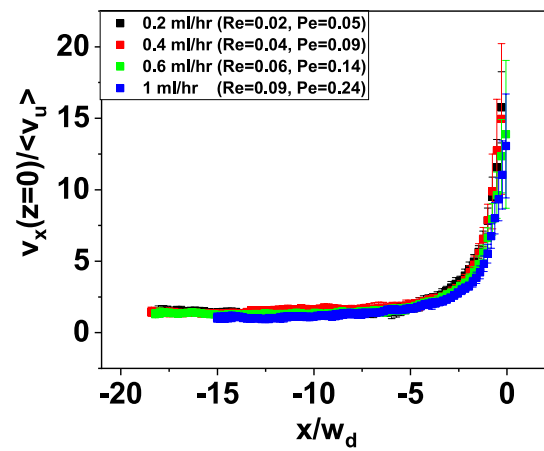


Fig. 6 The non-dimensionalized axial velocity profiles along the  $z = 0$  line measured for the 300 g/L BSA solution through the “26-G” microchannel for  $0.02 \leq Re \leq 0.09$ ,  $0.05 \leq Pe \leq 0.24$

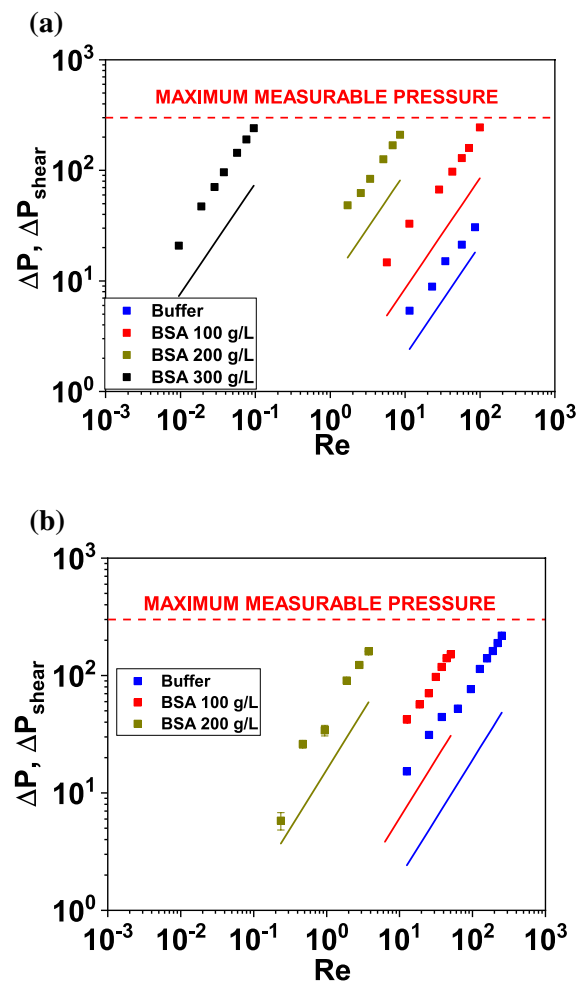
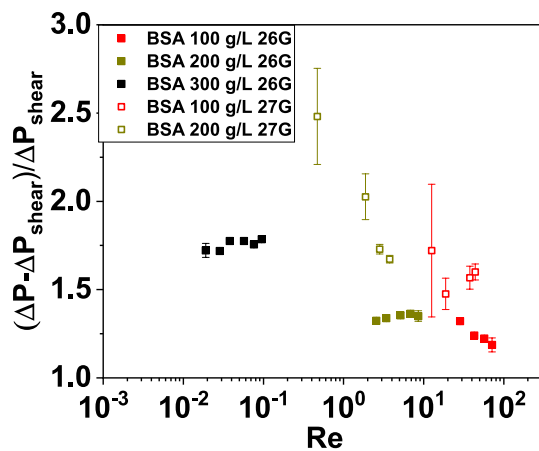


Fig. 7 The steady pressure drops through the “26-G” (a) and “27-G” (b) channels plotted as a function of  $Re$  for buffer and the BSA solutions. Symbols refer to experimental data points, and lines correspond to the analytical prediction as in Eqs. (7) and (8)



**Fig. 8** The non-dimensionalized extra pressure drop  $\Delta P' = \frac{\Delta P - \Delta P_{\text{shear}}}{\Delta P_{\text{shear}}}$  plotted as a function of  $Re$  for the flow of the BSA solutions through the “26-G” and the “27-G” channels

contraction, the difference between the total pressure drop and the purely shear contribution will be larger than in the case of Newtonian flows through hyperbolic contractions [41]. The extra pressure drop  $\Delta P' = \frac{\Delta P - \Delta P_{\text{shear}}}{\Delta P_{\text{shear}}}$  for the BSA solutions across the 26G and 27G flow geometries resulted to be within the range  $1.5 \leq \Delta P' \leq 3$  throughout the explored range of  $Re$  (see Fig. 8). The  $\Delta P'$  of the more viscous 300 g/L solution through the 26-G channel resulted larger than that of the other two solutions. Moreover, the  $\Delta P'$  of the 100 and 200 g/L solutions through the 27-G channel are above the corresponding values for the 26-G channel because the Hencky strain is larger for the 27G than for the 26G geometry. Note that the simulations carried out by Oliveira et al. [40] for planar contraction-expansion flows of Newtonian fluids show that the Couette correction (analogous to the  $\Delta P'$  defined here) increases sharply with  $Re$  for  $Re > 1$ . This is due to the fact that, differently than in the work by Oliveira et al., the flow geometries adopted here do not include an expansion part, where inertia-driven flow instabilities, which also cost nonlinearity in the pressure drop-flow rate curve, are typically observed.

Previous works [1, 15] do not consider the contribution to pressure drop due to extensional forces [21, 23] in modeling the injection force of dense protein solutions through syringes. More specifically, the authors assume that the total injection force is composed by only two components: an hydrodynamic contribution, which is based on purely shear forces, and a friction force which takes into account the interaction between plunger and syringe barrel. On the other hand, the results presented here suggest that the overall injection force of biopharmaceuticals through syringes also contains a contribution due to

purely extensional forces, which cannot be neglected in order for accurate predictions to be computed.

## 5 Conclusions

Using the microfluidic Rheo-Chip platform, the flow of concentrated ( $100 \text{ g/L} \leq c_2 \leq 300 \text{ g/L}$ ) BSA solutions under repulsive conditions was studied through shear, and contraction flows mimicking the typical geometry of syringes equipped with 26-G and 27-G needles. The shear viscosity retained a Newtonian behavior across the range of investigated shear rates ( $10 \text{ s}^{-1} \leq \dot{\gamma}, \eta_{\text{ext.}} \leq 10^4 \text{ s}^{-1}$ ), which was attributed to the Péclet number being below unity. Similarly, the flow of the 300 g/L BSA solution through the 26-G “syringe-on-chip” microdevices appeared to be Newtonian-like up to  $Pe = 0.24$ , which was likely because the BSA macromolecule retains its stability under the flow conditions imposed here [13].

Importantly, this work shows that the extensional viscosity of concentrated biopharmaceutical solutions also needs to be considered when one calculates the total force of syringe injection tests, because the measured pressure drop of the BSA solutions across the syringe-like microdevice resulted to be well above the purely shear contribution. This implies that the extensional viscosity plays an important role in determining the overall pressure drop of the complex flows underwent by protein solutions through needles, even if it is Newtonian. The extensional contributions are typically neglected in the formulation of predictions of injection forces [1, 7, 15, 48] and should then be considered if more realistic calculations have to be implemented.

Additionally, because the typical shear rate experienced by blood ranges from  $10 \text{ s}^{-1}$  in the ascending aorta [16] up to  $100 \text{ s}^{-1}$  in capillaries [25], while its  $\text{pH} \approx 7.4$  [55] is close to what probed here. Therefore, this work also indicates that human serum albumin maintains its native conformation under physiological flow conditions.

**Acknowledgements** This work was funded by the Biotechnology and Biological Sciences Research Council (BB/K011146). A. L. thanks Robin Curtis for useful discussions.

## Declarations

**Conflict of interest** The authors declare that they have no conflict of interest.

**Open Access** This article is licensed under a Creative Commons Attribution 4.0 International License, which permits use, sharing, adaptation, distribution and reproduction in any medium or format, as long as you give appropriate credit to the original author(s) and the source, provide a link to the Creative Commons licence, and indicate if changes were made. The images or other third party material in this

article are included in the article's Creative Commons licence, unless indicated otherwise in a credit line to the material. If material is not included in the article's Creative Commons licence and your intended use is not permitted by statutory regulation or exceeds the permitted use, you will need to obtain permission directly from the copyright holder. To view a copy of this licence, visit <http://creativecommons.org/licenses/by/4.0/>.

## References

- Allmendinger A, Fischer S, Huwlyer J, Mahler HC, Schwarb E, Zarraga IE, Mueller R (2014) Rheological characterization and injection forces of concentrated protein formulations: an alternative predictive model for non-newtonian solutions. *Eur J Pharm Biopharm* 87(2):318–328
- Amin S, Barnett GV, Pathak JA, Roberts CJ, Sarangapani PS (2014) Protein aggregation, particle formation, characterization & rheology. *Curr Opin Colloid Interface Sci* 19(5):438–449
- Arratia PE, Thomas C, Diorio J, Gollub JP (2006) Elastic instabilities of polymer solutions in cross-channel flow. *Phys Rev Lett* 96(14):144502
- Axelsson I (1978) Characterization of proteins and other macromolecules by agarose gel chromatography. *J Chromatogr A* 152(1):21–32
- Bekard IB, Asimakis P, Teoh CL, Ryan T, Howlett GJ, Bertolini J, Dunstan DE (2012) Bovine serum albumin unfolds in Couette flow. *Soft Matter* 8(2):385–389
- Binding D (1988) An approximate analysis for contraction and converging flows. *J Non-Newton Fluid Mech* 27(2):173–189
- Burckbuchler V, Mekhloufi G, Giteau AP, Grossiord J, Huille S, Agnely F (2010) Rheological and syringeability properties of highly concentrated human polyclonal immunoglobulin solutions. *Eur J Pharm Biopharm* 76(3):351–356
- Castellanos MM, Pathak JA, Colby RH (2014) Both protein adsorption and aggregation contribute to shear yielding and viscosity increase in protein solutions. *Soft Matter* 10(1):122–131
- Churchich JE (1962) Polarization of fluorescence studies of reduced bovine serum albumin. *Arch Biochem Biophys* 97(3):574–577
- De Gennes PG (1979) *Scaling concepts in polymer physics*. Cornell University Press
- Dear BJ, Hung JJ, Truskett TM, Johnston KP (2017) Contrasting the influence of cationic amino acids on the viscosity and stability of a highly concentrated monoclonal antibody. *Pharm Res* 34(1):193–207
- Dharmaraj VL, Godfrin PD, Liu Y, Hudson SD (2016) Rheology of clustering protein solutions. *Biomicrofluidics* 10(4):043509
- Dobson J, Kumar A, Willis LF, Tuma R, Higazi DR, Turner R, Lowe DC, Ashcroft AE, Radford SE, Kapur N, Brockwell DJ (2017) Inducing protein aggregation by extensional flow. *Proc Natl Acad Sci* 114(18):4673–4678. <https://doi.org/10.1073/pnas.1702724114>
- Fasano M, Curry S, Terreno E, Galliano M, Fanali G, Narciso P, Notari S, Ascenzi P (2005) The extraordinary ligand binding properties of human serum albumin. *IUBMB Life* 57(12):787–796
- Fischer I, Schmidt A, Bryant A, Besheer A (2015) Calculation of injection forces for highly concentrated protein solutions. *Int J Pharm* 493(1):70–74. <https://doi.org/10.1016/j.ijpharm.2015.07.054>
- Gabe IT, Gault JH, Ross JRJ, Mason DT, Mills CJ, Schillingford JP, Braunwald E (1969) Measurement of instantaneous blood flow velocity and pressure in conscious man with a catheter-tip velocity probe. *Circulation* 40(5):603–614
- Garidel P, Kuhn AB, Schäfer LV, Karow-Zwick AR, Blech M (2017) High-concentration protein formulations: how high is high? *Eur J Pharm Biopharm* 119:353–360
- Godfrin PD, Zarraga IE, Zarzar J, Porcar L, Falus P, Wagner NJ, Liu Y (2016) Effect of hierarchical cluster formation on the viscosity of concentrated monoclonal antibody formulations studied by neutron scattering. *J Phys Chem B* 120(2):278–291
- Gulati S, Liepmann D, Muller SJ (2008a) Elastic secondary flows of semidilute DNA solutions in abrupt 90 microbends. *Phys Rev E* 78(3):036314
- Gulati S, Muller SJ, Liepmann D (2008b) Direct measurements of viscoelastic flows of DNA in a 2: 1 abrupt planar micro-contraction. *J Non-Newton Fluid Mech* 155(1):51–66
- Haward SJ (2014) Characterization of hyaluronic acid and synovial fluid in stagnation point elongational flow. *Biopolymers* 101(3):287–305
- Haward SJ, McKinley GH (2012) Stagnation point flow of worm-like micellar solutions in a microfluidic cross-slot device: effects of surfactant concentration and ionic environment. *Phys Rev E* 85(3):031502
- Haward SJ, Odell JA, Berry M, Hall T (2011) Extensional rheology of human saliva. *Rheol Acta* 50(11–12):869–879
- Haward SJ, McKinley GH, Shen AQ (2016) Elastic instabilities in planar elongational flow of monodisperse polymer solutions. *Sci Rep* 6:1–18
- Ivanov K, Kalinina M, Levkovich YI (1981) Blood flow velocity in capillaries of brain and muscles and its physiological significance. *Microvascu Res* 22(2):143–155
- Jaishankar A, McKinley GH (2013) Power-law rheology in the bulk and at the interface: quasi-properties and fractional constitutive equations. *Proc R Soc A* 469:20120284
- Jaspe J, Hagen SJ (2006) Do protein molecules unfold in a simple shear flow? *Biophys J* 91(9):3415–3424
- Jorgensen L, Hostrup S, Moeller EH, Grohgan H (2009) Recent trends in stabilising peptides and proteins in pharmaceutical formulation—considerations in the choice of excipients. *Expert Opin Drug Deliv* 6(11):1219–1230
- Kanai S, Liu J, Patapoff TW, Shire SJ (2008) Reversible self-association of a concentrated monoclonal antibody solution mediated by Fab–Fab interaction that impacts solution viscosity. *J Pharm Sci* 97(10):4219–4227
- Lanzaro A, Yuan XF (2011) Effects of contraction ratio on non-linear dynamics of semi-dilute, highly polydisperse paam solutions in microfluidics. *J Non-Newton Fluid Mech* 166(17):1064–1075
- Lanzaro A, Yuan XF (2014) A quantitative analysis of spatial extensional rate distribution in nonlinear viscoelastic flows. *J Non-Newton Fluid Mech* 207:32–41
- Lanzaro A, Li Z, Yuan XF (2015) Quantitative characterization of high molecular weight polymer solutions in microfluidic hyperbolic contraction flow. *Microfluid Nanofluid* 18(5–6):819–828
- Lanzaro A, Corbett D, Yuan XF (2017) Non-linear dynamics of semi-dilute paam solutions in a microfluidic 3D cross-slot flow geometry. *J Non-Newton Fluid Mech* 242:57–65
- Larson RG (1999) *The structure and rheology of complex fluids*, vol 150. Oxford University Press, New York
- Li Z, Yuan XF, Haward SJ, Odell JA, Yeates S (2011) Non-linear dynamics of semi-dilute polydisperse polymer solutions in microfluidics: a study of a benchmark flow problem. *J Non-Newton Fluid Mech* 166(16):951–963
- Liu J, Nguyen MD, Andya JD, Shire SJ (2005) Reversible self-association increases the viscosity of a concentrated monoclonal antibody in aqueous solution. *J Pharm Sci* 94(9):1928–1940
- Mathaes R, Koulou A, Joerg S, Mahler HC (2016) Subcutaneous injection volume of biopharmaceuticals: pushing the boundaries. *J Pharm Sci* 105(8):2255–2259

38. Meinhart C, Wereley S, Gray M (2000) Volume illumination for two-dimensional particle image velocimetry. *Measur Sci Technol* 11(6):809–14
39. Meinhart CD, Wereley ST, Santiago JG (1999) PIV measurements of a microchannel flow. *Exp Fluids* 27(5):414–419
40. Oliveira MS, Rodd LE, McKinley GH, Alves MA (2008) Simulations of extensional flow in microrheometric devices. *Microfluid Nanofluid* 5(6):809
41. Oliveira MSN, Alves MA, Pinho FT, McKinley GH (2007) Viscous flow through microfabricated hyperbolic contractions. *Exp Fluids* 43(2–3):437–451
42. Pan W, Filobelo L, Pham ND, Galkin O, Uzunova VV, Vekilov PG (2009) Viscoelasticity in homogeneous protein solutions. *Phys Rev Lett* 102(5):058101
43. Patel AR, Kerwin BA, Kanapuram SR (2009) Viscoelastic characterization of high concentration antibody formulations using quartz crystal microbalance with dissipation monitoring. *J Pharm Sci* 98(9):3108–3116
44. Pathak JA, Hudson SD (2006) Rheo-optics of equilibrium polymer solutions: wormlike micelles in elongational flow in a microfluidic cross-slot. *Macromolecules* 39(25):8782–8792
45. Perkins TT, Smith DE, Chu S (1997) Single polymer dynamics in an elongational flow. *Science* 276(5321):2016–2021
46. Pipe CJ, Majmudar TS, McKinley GH (2008) High shear rate viscometry. *Rheol Acta* 47(5–6):621–642
47. Ramallo N, Paudel S, Schmit J (2019) Cluster formation and entanglement in the rheology of antibody solutions. *J Phys Chem B* 123(18):3916–3923
48. Rathore N, Pranay P, Bernacki J, Eu B, Ji W, Walls E (2012) Characterization of protein rheology and delivery forces for combination products. *J Pharm Sci* 101(12):4472–4480
49. Rodd L, Cooper-White J, Boger D, McKinley G (2007) Role of the elasticity number in the entry flow of dilute polymer solutions in micro-fabricated contraction geometries. *J Non-Newton Fluid Mech* 143(2):170–191
50. Rodd LE, Scott TP, Boger DV, Cooper-White JJ, McKinley GH (2005) The inertio-elastic planar entry flow of low-viscosity elastic fluids in micro-fabricated geometries. *J Non-Newton Fluid Mech* 129(1):1–22
51. Roos M, Ott M, Hofmann M, Link S, Rossler E, Balbach J, Krushelnitsky A, Saalwachter K (2016) Coupling and decoupling of rotational and translational diffusion of proteins under crowding conditions. *J Am Chem Soc* 138(32):10365–10372
52. Santiago JG, Wereley ST, Meinhart CD, Beebe D, Adrian RJ (1998) A particle image velocimetry system for microfluidics. *Exp Fluids* 25(4):316–319
53. Sarangapani PS, Hudson SD, Migler KB, Pathak JA (2013) The limitations of an exclusively colloidal view of protein solution hydrodynamics and rheology. *Biophys J* 105(10):2418–2426
54. Schneider S, Nuschele S, Wixforth A, Gorzelanny C, Alexander-Katz A, Netz R, Schneider M (2007) Shear-induced unfolding triggers adhesion of von willebrand factor fibers. *Proc Natl Acad Sci* 104(19):7899–7903
55. Severinghaus J (1958) Oxyhemoglobin dissociation curve correction for temperature and pH variation in human blood. *J Appl Physiol* 12(3):485–486
56. Shah M, Corbett D, Lanzaro A, Roche A, Sibanda N, Davis P, Uddin S, van der Walle C, Curtis R, Pluen A (2020) Micro-and macroviscosity relations in high concentration antibody solutions. *Eur J Pharm Biopharm* 153:211–221
57. Sharma V, Jaishankar A, Wang YC, McKinley GH (2011) Rheology of globular proteins: apparent yield stress, high shear rate viscosity and interfacial viscoelasticity of bovine serum albumin solutions. *Soft Matter* 7(11):5150–5160
58. Shire SJ, Shahrokh Z, Liu J (2004) Challenges in the development of high protein concentration formulations. *J Pharma Sci* 93(6):1390–1402
59. Sønderby P, Bukrinski JT, Hebditch M, Peters GH, Curtis RA, Harris P (2018) Self-interaction of human serum albumin: a formulation perspective. *ACS Omega* 3(11):16105–16117
60. Szymczak P, Cieplak M (2006) Stretching of proteins in a uniform flow. *J Chem Phys* 125(16):164903
61. Szymczak P, Cieplak M (2007) Proteins in a shear flow. *J Chem Phys* 127(15):10B618
62. Viola M, Sequeira J, Seiça R, Veiga F, Serra J, Santos AC, Ribeiro AJ (2018) Subcutaneous delivery of monoclonal antibodies: how do we get there? *J Controll Release* 286:301–314
63. Wang WH, Lilyestrom WG, Hu ZY, Scherer TM (2018) Cluster size and quinary structure determine the rheological effects of antibody self-association at high concentrations. *J Phys Chem B* 122(7):2138–2154
64. White FM, Corfield I (2006) *Viscous fluid flow*, vol 3. McGraw-Hill Higher Education, Boston
65. Yadav S, Sreedhara A, Kanai S, Liu J, Lien S, Lowman H, Kalonia DS, Shire SJ (2011) Establishing a link between amino acid sequences and self-associating and viscoelastic behavior of two closely related monoclonal antibodies. *Pharm Res* 28(7):1750–1764
66. Yentis SM, Hirsch NP, Ip J (2018) *Anaesthesia and intensive care AZ E-book: an encyclopaedia of principles and practice*. Elsevier Health Sciences
67. Yuan Xf (2016) Rheometry apparatus. US Patent 9,354,152
68. Zarraga IE, Taing R, Zarzar J, Luoma J, Hsiung J, Patel A, Lim FJ (2013) High shear rheology and anisotropy in concentrated solutions of monoclonal antibodies. *J Pharm Sci* 102(8):2538–2549
69. Zhao Y, Cheung P, Shen AQ (2014) Microfluidic flows of wormlike micellar solutions. *Adv Colloid Interface Sci* 211:34–46

**Publisher's Note** Springer Nature remains neutral with regard to jurisdictional claims in published maps and institutional affiliations.